JOURNAL OF SPACECRAFT AND ROCKETS
Vol. 40, No. 6, November–December 2003

Optimal Active Control of Launch Vibrations of Space Structures

Ratneshwar Jha,* Matthew Pausley,† and Goodarz Ahmadi‡
Clarkson University, Potsdam, New York 13699

Vibration reduction of space structures during launch is investigated experimentally. An optimal control law is formulated, based on a lumped parameter state-space model of the structure. A single piezoelectric actuator is bonded to the surface near the base to provide actuation. Band-limited white noise and recorded space shuttle launch excitations are used to assess the performance of the control system. Significant reductions in the vibrations are obtained using very low actuator power. The study indicates a large potential for improvements in payload protection during the space shuttle liftoff by using smart-structures technology.

Nomenclature

A = system matrix
A_a = cross-sectional area of actuator, m^2
A_b = cross-sectional area of beam (wall), m^2
B = input matrix
B_c = control effect matrix
$\boldsymbol{b}$ = $[1\ \ 1\ \ 1]^T$
b_a = actuator width, m
C = damping matrix, N/(m $\cdot$ s^{-1})
C_a = actuator capacitance, F
C_y = output matrix
d_{31} = piezoelectric strain coefficient, m/V
E = disturbance matrix
E_a = Young's modulus of actuator material, Pa
E_w = Young's modulus of wall material, Pa
F_b = block force, N
G = control gain matrix
g = acceleration due to gravity (9.8 m/s^2)
I = identity matrix
I_w = second moment of area of wall cross section, m^4
J = performance index
K = stiffness matrix, N/m
k_w = stiffness constant, N/m
L = output injection matrix
l_w = distance between levels, m
M = mass matrix, kg
O = observability matrix
P = solution of algebraic Riccati equation
P_{act} = actuator power consumption, W
Q = state weighting matrix
R = control weighting matrix
t = time, s
t_a = actuator thickness, m
$\boldsymbol{u}$ = control force, N
V = applied voltage, V
$\boldsymbol{x}$ = displacement vector, m
$\bar{\boldsymbol{x}}$ = state vector
$\ddot{\boldsymbol{x}}_a$ = absolute acceleration, m/s^2
$\ddot{\boldsymbol{x}}_b$ = base acceleration, m/s^2
$\hat{\boldsymbol{x}}$ = estimated state vector
$\boldsymbol{y}$ = output vector
$\alpha_e(A)$ = desired estimator poles
$\varepsilon_{\max}$ = maximum induced strain
ρ = structural constant
ω = excitation frequency, rad/s

Presented as Paper 2002-1628 at the 43rd Structures, Structural Dynamics, and Material Conference, Denver, CO, 22–25 April 2002; received 7 August 2002; revision received 2 April 2003; accepted for publication 29 April 2003.

*Assistant Professor, Department of Mechanical and Aeronautical Engineering; ratan@clarkson.edu. Senior Member AIAA.
†Graduate Student, Department of Mechanical and Aeronautical Engineering; currently Engineer, PGT–Aerodynamic Design, General Electric Power Systems, 1 River Road, Building 81N-100, Schenectady, NY 12345.
‡Professor, Department of Mechanical and Aeronautical Engineering.

Introduction

TO exploit the full benefits of microgravity environment in space, many types of experimental equipment must be transported aboard the space shuttle or aboard expendable rockets. An obvious obstacle to the design of any orbital experiment is the amount of potentially harmful vibrations that are encountered during launch and landing. Similarly, vibrations during space shuttle liftoff are known to affect greatly the design of satellites or other sensitive equipment. Thus, vibration suppression is very important for avoiding failure and for increasing payload mass. However, it is a challenging task to overcome vibration damage to sensitive equipment during launch.

Several researchers have investigated passive vibration isolation of payload during liftoff. Lee-Glauser and Ahmadi[1] extensively studied base isolation for satellite subsystems and generalized space shuttle payloads. Shimmel[2] studied the use of laminated rubber bearings for the protection of a generic space structure subject to space shuttle takeoff accelerations. Passive control methods to isolate spacecraft and Space Shuttle payloads during launch have been flight-tested successfully.[3] Lee-Glauser et al.[4] investigated the effectiveness of an active vibration absorber theoretically by using a lumped-parameter model of the system. However, no experimental investigation has been reported for active vibration control during space shuttle (or expendable rocket) liftoff.

The real-time sensing and actuation capabilities of smart structures provide a powerful means for active vibration control of space structures. A smart structure involves the integration of a physical structure with distributed active (or smart) material-based actuators and sensors and a controller that analyzes sensor responses and commands the actuators. A smart structure has the ability to modify the response of the system to external or internal disturbances in a desired manner. Crawley and de Luis[5] suggested the use of piezoelectric actuators as elements of structures with highly distributed actuators, sensors and processing networks. Currently, most piezoelectric devices use lead zirconate titanate (PZT), which is a piezoceramic material. Sater and Crowe[6] discuss the current state of development of PZT actuators. Chopra[7] presents the characteristics of piezoelectric materials, their constitutive relations, structural modeling, and some applications. Although PZT actuators generate low strains, a wide range of actuation frequency (large bandwidth), low cost, lightweight, and easy integration make them highly suitable for vibration, aeroelastic, and aerodynamic control applications. Vibration suppression of flexible beams, plates, and other structures by using PZT actuators has been investigated by a number of researchers.[8–11]

A large number of theoretical and experimental investigations have been reported for spacecraft vibration suppression using smart structures in the microgravity environment.[12,13] However, the use of smart structures for active vibration control during launch appears to be absent from the literature. This paper presents the development and experimental validation of an optimal control system for minimizing launch-type vibrations of payload by using smart-structures technology. A single PZT actuator is bonded to the sidewall of a three-level structure (representing equipment housing) to provide the control force. A theoretical model of the structure is derived for control-law development using lumped-parameter equations of motion and state-space modeling concepts. The control law is based on output (acceleration) feedback, combined with an estimator to generate the full state. The ability of the control system to reduce the vibrations of the structure is quantified experimentally for various base excitations. The following section contains the formulation of the equations that govern the response of the three-level structure. Then, the optimal control-law development, details of experimental setup, and results are presented and discussed.

Equations of Motion

The equations of motion are based on a linear, lumped-mass model and include the base accelerations. Figure 1 shows the structural model and lumped-mass approximation for the three-level structure used in the present research. The effective mass of each level is obtained by summing the mass for that level and half the mass of the walls surrounding that level. The complete structural mass is accounted for by including mass contributions from the walls, which improves the structural model. The walls between each level are assumed to act as bending elements in the direction of excitation. The general equations of motion for the structure are given as

$$M\ddot{\boldsymbol{x}} + C\dot{\boldsymbol{x}} + K\boldsymbol{x} = -M\boldsymbol{b}\ddot{x}_b + B_c\boldsymbol{u} \tag{1}$$

where M, C, and K represent 3×3 mass, damping, and stiffness matrices of the structure, respectively. The three-dimensional vector $\boldsymbol{x}$ represents the displacements of each level, relative to the base. The 3×1 vector $\boldsymbol{b}$ reflects the effect of base acceleration $\ddot{x}_b$ on each level. The 3×3 matrix B_c is the control-effect matrix, and the 3×1 vector $\boldsymbol{u}$ is the control force. Because only one actuator is bonded between the base and the first level of the structure, the first element of the control-effect matrix is unity, and the remaining elements are zero. Similarly, only the first term of the control-input vector is nonzero.

The shear-stiffness constant is calculated by using a fixed–fixed beam condition because the wall and the adjacent levels are rigidly connected. The shear-stiffness constant is given by the following equation:

$$k_w = 12E_wI_w/l_w^3 \tag{2}$$

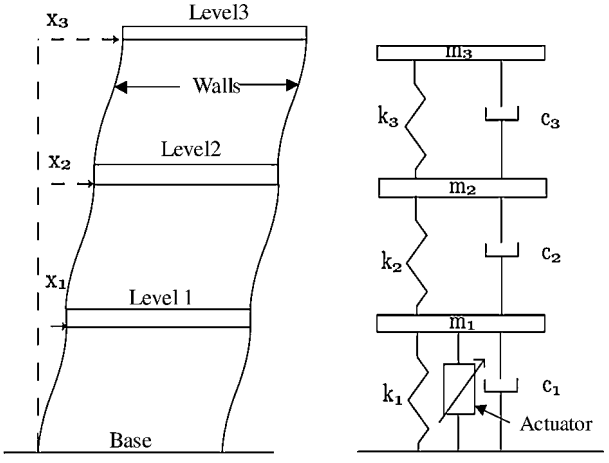

a) Three-level structure **b) Lumped-mass model**

Fig. 1 Three-level structure and lumped-mass approximation.

Because the structure has two walls that act as parallel springs, the total stiffness constant is twice that given by Eq. (2). To evaluate the damping matrix, the structure is assumed to exhibit a proportional damping, and the modal damping ratios are calculated from the experimental data by using the quadrature peak picking method.[14]

State-space techniques are used in the present study to solve the equations of motion. The state-space representation of the system is defined by the following state and output equations:

$$\dot{\bar{\boldsymbol{x}}} = A\bar{\boldsymbol{x}} + B\boldsymbol{u} + E\ddot{\boldsymbol{x}}_b, \qquad \boldsymbol{y} = C_y\bar{\boldsymbol{x}} \tag{3}$$

The state vector $\bar{\boldsymbol{x}} = [x_1 \;\; x_2 \;\; x_3 \;\; \dot{x}_1 \;\; \dot{x}_2 \;\; \dot{x}_3]^T$ consists of the displacements and velocities at each level. In general state-space formulations, the output $\boldsymbol{y}$ is a function of the state vector and the control-input vector. To simplify further developments, the output is formulated as a function of the state vector only, by following the approach adopted by Spencer et al.[15] Rewriting Eq. (1), the absolute acceleration $\ddot{\boldsymbol{x}}_a$ (which is measured by the accelerometers attached to each level) is given by

$$\ddot{\boldsymbol{x}}_a = -M^{-1}K\boldsymbol{x} - M^{-1}C\dot{\boldsymbol{x}} + M^{-1}B_c\boldsymbol{u} \tag{4}$$

Subtracting the term $M^{-1}B_c\boldsymbol{u}$ from the measured absolute accelerations results in the output given by Eq. (3) with

$$A = \begin{bmatrix} 0 & I \\ -M^{-1}K & -M^{-1}C \end{bmatrix}, \qquad B = \begin{bmatrix} 0 \\ M^{-1}B_c \end{bmatrix}$$

$$C_y = [-M^{-1}K \quad M^{-1}C], \qquad E = \begin{bmatrix} 0 \\ -\boldsymbol{b} \end{bmatrix} \tag{5}$$

The system matrix A, input matrix B, disturbance matrix E, and output matrix C_y are determined by the (modeled) properties of the system. Model performance is highly dependent on knowledge of the system. Measurement uncertainty in the masses and mathematical errors in determining stiffness constants, for example, affect the prediction of response to a given input.

Optimal Control

The control law is developed by using the standard linear quadratic regulator (LQR) optimal-control technique.[16] The control-input vector $\boldsymbol{u}$ is obtained from

$$\boldsymbol{u} = -G\bar{\boldsymbol{x}} \tag{6}$$

where G is the control gain matrix. Equation (6) is known as the control law. An LQR controller design involves a compromise between the conflicting goals of high performance (low accelerations) and minimum applied control force. Controller development begins by first defining a quadratic performance index (where the prime indicates transpose)

$$J = \int_0^\infty (\bar{\boldsymbol{x}}'Q\bar{\boldsymbol{x}} + \boldsymbol{u}'r\boldsymbol{u})\,\mathrm{d}t \tag{7}$$

where Q and R are real symmetric weighting matrices that allow priority to be allocated between the states and the control effort required. Because the states and inputs are squared in Eq. (7), minimization of the performance index leads to minimum energy in the system.

Following the optimal-control formulation, the control gain matrix is given by

$$G = -R^{-1}B'P \tag{8}$$

where P is the solution of the following algebraic Riccati equation:

$$A'P + PA + Q - PBR^{-1}B'P = 0 \tag{9}$$

When this formulation is used, G is a steady-state gain matrix that can be computed before implementing the control law. Simulations

are then used to assess the performance of the controller before it is validated experimentally.

Inspection of Eq. (6) indicates that the feedback control law relies on the full-state vector $\bar{\boldsymbol{x}}$ to be fed back through G, which is known as full-state feedback. However, the control system developed in the present study utilizes the measured accelerations, which is known as output feedback. To obtain the states from the measured output $\boldsymbol{y}$, an estimator is formulated that gives an estimate of the unknown states $\hat{\boldsymbol{x}}$. The control law then becomes

$$\boldsymbol{u} = -G\hat{\boldsymbol{x}} \tag{10}$$

where $\hat{\boldsymbol{x}}$ is the estimated state vector. An estimator is formulated as a dynamic system, which has a form very similar to the system model. Accordingly, the estimator dynamics are given by

$$\dot{\hat{\boldsymbol{x}}} = A\hat{\boldsymbol{x}} + B\boldsymbol{u} + L(\boldsymbol{y} - C_y\hat{\boldsymbol{x}}) \tag{11}$$

where the output injection matrix L is selected to achieve satisfactory estimation. In Eq. (11), the estimated state $\hat{\boldsymbol{x}}$ is fed back through the C_y matrix to generate an estimated acceleration. The quantity $C_y\hat{\boldsymbol{x}}$ is then subtracted from the actual output $\boldsymbol{y}$ to create an error signal. If designed properly, the dynamics of the estimator drive the error signal to zero, thereby creating an accurate estimate of the unknown states.

The output injection matrix is determined using Ackermann's formula (see Ref. 17) as follows:

$$L = \alpha_e(A)\,O^{-1}[0 \quad 0 \quad 0 \quad 0 \quad 0 \quad 1] \tag{12}$$

In Eq. (12), $\alpha_e(A)$ are the desired estimator poles given the system matrix A and O is the observability matrix. To reduce the estimation error to zero quickly, the estimator poles must be far to the left of the system poles in the s plane. For this study, the estimator yielded excellent performance when its poles were placed 10 time constants farther than the poles of the dynamic system represented by system matrix A.

Piezoelectric Actuation

When a piezoelectric material is stressed mechanically by a force, it generates an electric charge potential. Conversely, when an electric field is applied across the thickness of the material, it elongates or shortens depending on the polarity of the applied electric field. Thus, a piezoelectric element is capable of being used both as actuator and sensor. When attached to a host structure, piezoelectric actuators cause deformation of the structure. In the current research, the control force is generated by a single PZT actuator that is modeled by using a simple block-force method, as presented by Chopra.[7] This model assumes that a rectangular actuator is perfectly bonded to an isotropic beam, such as the wall of the structure shown in Fig. 2. If a voltage V is applied across the two sides of the actuator having thickness t_a, the maximum induced strain (or free strain) is given by

$$\varepsilon_{\max} = d_{31}(V/t_a) \tag{13}$$

where d_{31} is the piezoelectric strain coefficient. Thus, the amount of strain is dependent on the voltage, whereas the direction of strain is dependent on polarity. An actuator generates the maximum amount of force under the zero strain condition. This maximum amount of force, called block force, is given by

$$F_b = d_{31}E_a b_a V \tag{14}$$

The actual amount of force induced in the beam (for a given voltage V) is a function of the block force and physical properties of the actuator and the host beam. The induced force is given by

$$F = d_{31}E_a b_a V \frac{E_b A_b}{E_b A_b + E_a A_a} \equiv \rho V \tag{15}$$

The constant ρ is determined by the material and geometric properties of the actuator and the host structure. To implement the control law of Eq. (10), the matrix B_c is multiplied by ρ and the actuator voltage is obtained from the following equation:

$$V = -G\hat{\boldsymbol{x}} \tag{16}$$

The state-space model of the structure (including the actuator) is used for calculating the control gain matrix G and output injection matrix L. Thus, the developed theoretical model is used only to determine the optimal actuator voltage V, given the measured accelerations at the three levels. The structural response to the excitations and piezoelectric actuation (for the applied voltage) presented are based on experimental measurements.

The power consumption of the actuators depends mostly on piezoelectric material properties and actuation voltage, and the dynamics of the controlled structure may be ignored for a conservative estimate.[18] For a sinusoidal actuation voltage $V\sin(\omega t)$ and actuator capacitance C_a, the actuator power consumption is obtained from

$$P_{\text{act}} = \omega C_a V^2/2 \tag{17}$$

Experimental Setup

The central piece of the experiment is a three-level structure (Fig. 2) fabricated entirely from 6061 aluminum. Each of the levels is 76.2 cm^2 square with a thickness of 0.635 cm. A fourth level with identical dimensions connects the walls at the base. Each level has a mass of 0.104 kg. The levels are attached to the sidewalls (with three 4–40 screws on each side) such that the distance between the levels is equal. The sidewalls are 31.1 cm tall, 7.62 cm wide, and 0.09 cm thick. The mass of each side wall is 0.067 kg. The structure is bolted through the base to a moving plate. The plate is 15.2 cm^2 in area and 1.27 cm thick. Ball bearings mounted to the plate allow it to move freely upon a fixed base that is securely mounted to the test bench. When grooves machined into the fixed base are used, the moving plate can only move in one direction. The moving plate is made heavier than the three-level structure by the addition of three large steel pieces to the underside to model more realistically the actual equipment attached to the space shuttle. (The vertical plates shown in Fig. 2 by the side of the structure support the wiring.)

A 15-cm-long rod of 0.63-cm diam connects the moving plate to an electromagnetic shaker. The shaker is relatively small, with diameter of 14.9 cm and a length of 14.3 cm. The maximum displacement is 0.8 cm peak to peak, and the maximum acceleration (without load) is 75 g. According to the manufacturer, the usable bandwidth of the shaker is between 10 Hz and 20 kHz.

A single PZT actuator was bonded to the surface of the right wall near the root to provide the actuation force. For a single actuator, this location has been shown to be optimal for vibration suppression.[9] The actuator dimensions are 5.08 cm long, 3.81 cm wide, and 0.038 cm thick. The actuator has a voltage range of $\pm$200 V, capacitance of 0.1 μF, and the piezoelectric strain

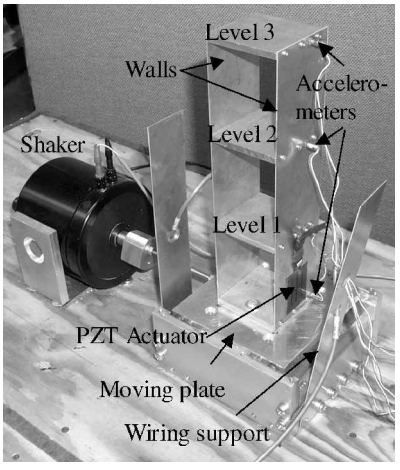

Fig. 2 Experimental setup.

coefficient $d_{31} = -179 \times 10^{-10}$ cm/V. The actuator was bonded to the structure by using a two-part epoxy, with a 24-h cure time, and vacuum bagging.

Accelerometers are attached at each level and the base to translate the acceleration of the structure into voltage signals. Each accelerometer has a mass of 2 g and is 1.37 cm in diameter. The sensitivity of the accelerometers lies between 100 and 110 mV/g. A signal conditioner amplifies this signal before low-pass filters process the signal. The filters attenuate any signal above 150 Hz to prevent aliasing. The accelerometer signals are then used as inputs in the optimal control system implemented on a Windows-based workstation. A data acquisition board (DAQ) is used for communication between the workstation and other equipment. The actuation command signal generated by the computer is amplified by gain circuitry and a high-voltage amplifier before feeding to the actuator. A schematic diagram of the experimental setup is shown in Fig. 3.

Results and Discussion

The natural frequencies of the structure were obtained by exciting the first three modes by using a white-noise base excitation (Fig. 4).

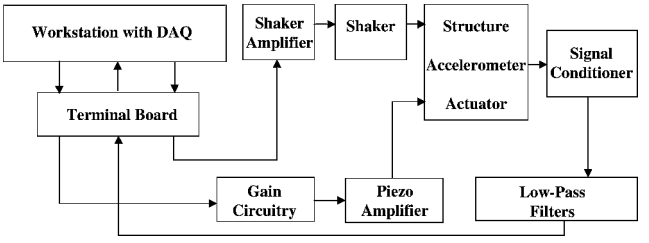

Fig. 3 Schematic diagram of the experimental setup.

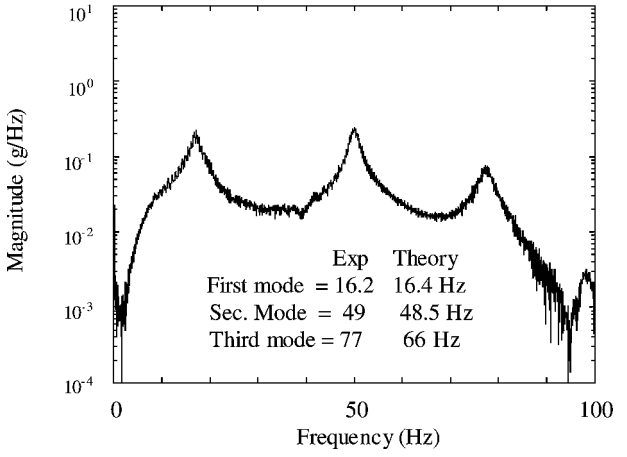

Fig. 4 Natural frequencies.

The first three natural frequencies occur at 16.2, 49, and 77 Hz. This preliminary characterization of the structural dynamics served as a guide for the development of the state-space model. Substitution of the system parameters into the state-space representation of the structure predicted natural frequencies of 16.4, 48.5, and 66 Hz. Excellent agreement is found for the first and second modes, but the third mode does not match closely. However, because most of the energy of the structure is contained in the lower modes, it is concluded that the state-space model is a reasonable representation of the structure.

The present paper focuses on experimental results for white noise and space shuttle launch-type excitation signals and the actuator power requirements. Pausley[19] presents additional results including the controlled and uncontrolled responses of the structure for sinusoidal excitations and comparisons between theoretical predictions and experimental results.

White Noise Base Excitation

Band-limited white noise in the range of 0–100 Hz was sent to the shaker to excite the structure. Figure 5 shows the time history and frequency content of the white-noise test signal measured by the base accelerometer at 2000-Hz sampling rate. The test signal generated peak accelerations of about ± 0.35 g. The intensity of the noise was set such that the magnitude of the accelerance frequency-response function was constant at approximately 0.02, at frequencies above 20 Hz. The frequency response of the shaker reduces below 20 Hz and shows a marked decline below 10 Hz (Fig. 5), indicating the limitation of the shaker to reproduce the commanded accelerations at lower frequencies. The white-noise excitation includes all of the first three natural frequencies of the structure, although the contribution of the first mode (at 16.2 Hz) is somewhat reduced due to the reduction in the response of the shaker.

The uncontrolled and controlled response of each of the three levels of the structure for the white-noise base excitation is shown in Fig. 6. The third-level response shows the largest peak and root-mean-square (rms) vibrations. The optimal control system (employing a single PZT actuator) reduces the first-level rms accelerations from 0.104 to 0.084 g, which is a decrease of 19%. Similarly, the second-level rms accelerations show a reduction by 17.5%, decreasing from 0.094 to 0.077 g. The most critical third-level vibrations show a slightly larger improvement of 20%, lowering the rms value from 0.135 to 0.108 g. The magnitude of the peak acceleration for the third level is also reduced from approximately 0.5 to 0.4 g.

Filtered STS 41 Excitation

STS 41 was launched from Cape Canaveral, Florida, in 1990. Triaxial accelerometers mounted on the floor of the cargo bay recorded the accelerations during liftoff. For this study, the acceleration time history for the Z direction (where X and Y axes are along fuselage and wing span, respectively) is used as a test input. Although the X- and Y-direction records are also available, both contain a nonzero mean that is, a velocity, which make them unsuitable as

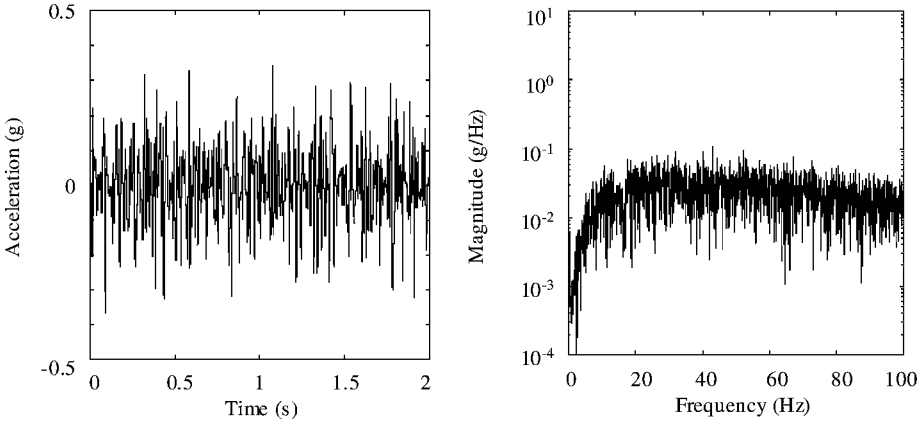

Fig. 5 White-noise test signal.

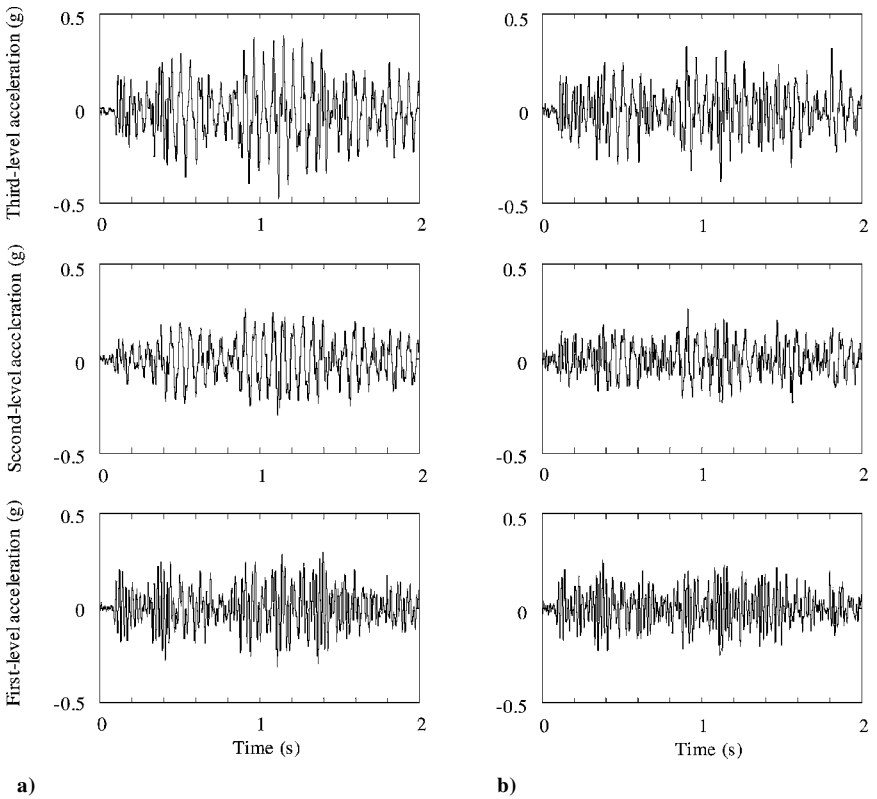

Fig. 6 Response to white-noise base excitation: a) uncontrolled and b) controlled.

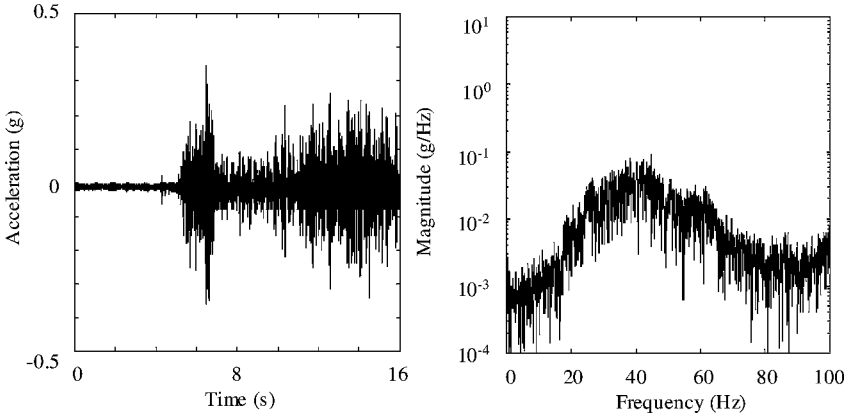

Fig. 7 Filtered STS 41 *Z*-direction acceleration (courtesy of NASA).

inputs. Because of the reduced response of the shaker at frequencies below 20 Hz, the STS 41 accelerations were filtered to include disturbances between 25 and 150 Hz only. The time history and frequency content of the filtered *Z*-direction accelerations are given in Fig. 7. During liftoff, the accelerations oscillate between ± 0.4 *g* at high frequencies. The frequency content of the signal is focused around 35–50 Hz.

The second natural frequency (49 Hz) lies within the range mentioned, whereas the first and third natural frequencies (16.2 and 77 Hz, respectively) are clearly outside. Thus, the filtered STS 41 signals excite mainly the second mode of the structure. Figure 8 shows the uncontrolled and controlled vibrations of each of the three levels due to filtered STS 41 excitations. Modal analysis using the lumped-mass model indicates that the node line for the second mode lies slightly above the second level. Accordingly, the second-level response is very small, and its rms value remains unchanged. The third-level rms acceleration reduces from 0.113 to 0.102 *g*, which is a decrease of 10%. The largest rms accelerations are recorded for the first level. The closed-loop control shows a significant improvement of 13%, reducing the first-level rms vibrations from 0.122 to 0.105 *g*.

Actuator Power Requirements

Because the availability of power for control actuation is at a premium for most practical situations, it is important to quantify the power requirements. Several measurements were made using two different amplifiers powering the actuator. The low-voltage amplifier was limited to 50 V, and the high-voltage amplifier was used up to 200 V. (For all other results presented earlier, the high-voltage amplifier was used.) For these tests, the signal issued from the DAQ was held constant as commanded by the optimal control system. However, the gain circuitry was used to modulate the command voltage sent to the actuator. Base excitation at the first natural frequency (16.2 Hz) was used to evaluate the power requirements. Frequency response of the command signal showed that the actuator voltage had the same frequency as the excitation. The percentage reduction in the third-level rms acceleration was used as the performance criterion.

The average actuator power was calculated using the recorded voltage and current for each test. Figure 9 shows the relationship between actuator power and control system performance. The active-control system delivers excellent performance, using very low power. The third-level rms acceleration is reduced by 24% (with

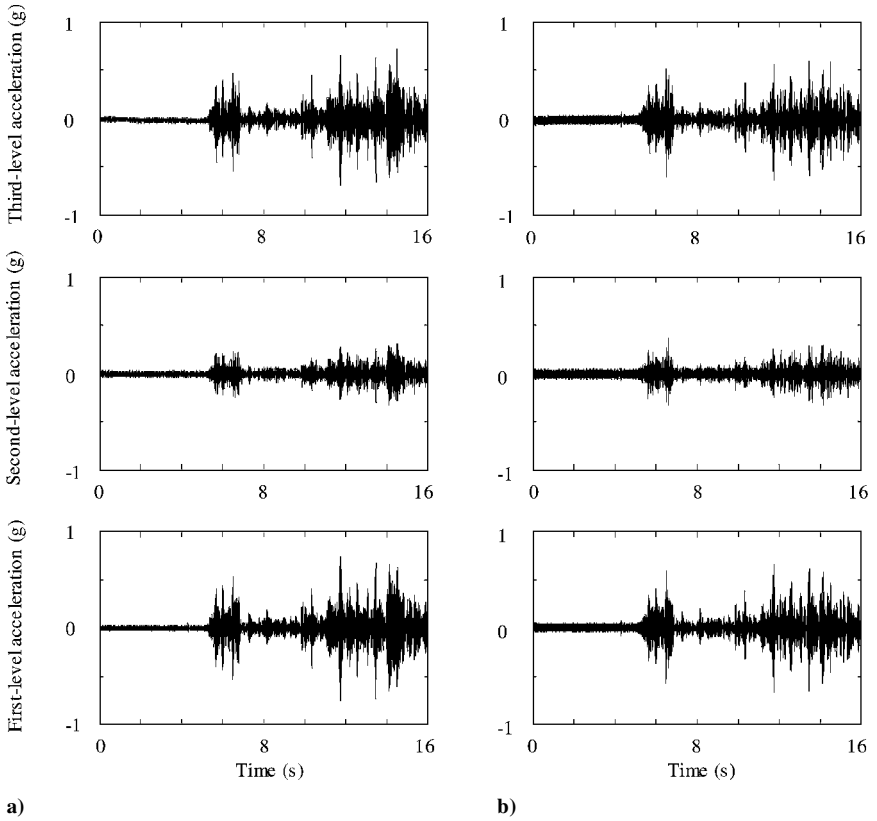

Fig. 8 Response to filtered STS 41 base excitation: a) uncontrolled and b) controlled.

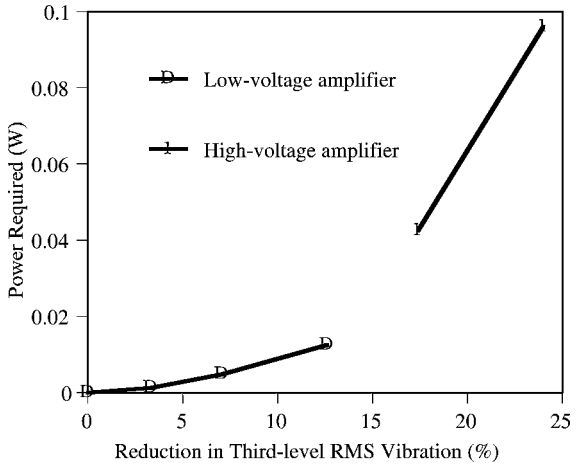

Fig. 9 Actuator power requirement vs rms vibration reduction.

the actuator voltage of 140 V), using the average power of 0.096 W. Theoretical calculation using Eq. (17) gives the power consumption of 0.1 W. For practical applications, a number of PZT actuators may be used (possibly combined with passive isolation) for protection from harmful vibrations leading to improved payload performance and reduced cost.

Conclusions

The development and evaluation of a smart-structure-based, optimal-control system for the suppression of payload vibrations during space shuttle liftoff has been presented. A three-level experimental structure that represents a payload housing and that has a moving base attached to a shaker has been examined. A lumped-parameter numerical model that was developed for the structure has also been discussed. Moreover, an optimal controller that is based on LQR concepts and a state estimator to allow output (acceleration) feedback has been presented. A single piezoelectric actuator bonded to the wall of the structure near the root has been used to provide the control force.

The results presented show that active control system reduces launch-type vibrations significantly, using very low power. In particular, rms vibrations are reduced by 17–20% for the band-limited (0–100 Hz) white-noise excitations. For the filtered STS 41 liftoff disturbances, first- and third-level accelerations are reduced by 13 and 10%, respectively. Less than 0.1 W of actuator power was consumed to reduce the third-level vibrations by 24% when the structure was excited at its first natural frequency. This study clearly indicates a large potential for reduction in space shuttle launch vibrations by using smart-structures technology. However, further research and development is necessary to address issues such as actuator scaling and practical implementation.

References

[1]Lee-Glauser, G., and Ahmadi, G., "Dynamic Response Spectra for an Aerospace Payload and Its Attachments," *Journal of Spacecraft and Rockets*, Vol. 30, No. 6, 1993, pp. 784–786.

[2]Shimmel, J. T., "Passive Vibration Control of Space Structures for Space Shuttle Liftoff, Descent, and Microgravity Environments," M.S. Thesis, Dept. of Mechanical and Aeronautical Engineering, Clarkson Univ., Potsdam, NY, Dec. 1999.

[3]Denoyer, K. K., and Johnson, C. D., "Recent Achievements in Vibration Isolation Systems for Space Launch and On-Orbit Applications," 52nd International Astronautical Congress, Paper IAF-01-I.2.01, Oct. 2001.

[4]Lee-Glauser, G., Ahmadi, G., and Layton J. B., "Satellite Active and Passive Vibration Control During Liftoff," *Journal of Spacecraft and Rockets*, Vol. 33, No. 3, 1996, pp. 428–432.

[5]Crawley, E. F., and de Luis, J., "Use of Piezoelectric Actuators as Elements of Intelligent Structures," *AIAA Journal*, Vol. 25, No. 10, 1987, pp. 1373–1385.

[6]Sater, J. M., and Crowe, C. R., "Smart Air and Space Structure Demonstrations: Status and Technical Issues," AIAA Paper 2000-1625, April 2000.

[7]Chopra, I., *Review of Current Status of Smart Structures and Integrated Systems: Proceedings of the SPIE—The International Society for Optical Engineering*, Vol. 2717, Society of Photo-Optical Instrumentation Engineers (International Society for Optical Engineering), Bellingham, WA, 1996, pp. 20–62.

[8]Chandrashekhara, K., and Agarwal, A. N., "Active Vibration Control of Laminated Composite Plates Using Piezoelectric Devices: A Finite Element Approach," *Journal of Intelligent Material Systems and Structures*, Vol. 4, No. 4, 1993, pp. 496–508.

[9]Chattopadhyay, A., Seeley, C. E., and Jha, R., "Aeroelastic Tailoring Using Piezoelectric Actuation and Hybrid Optimization," *Smart Materials and Structures*, Vol. 8, No. 1, 1999, pp. 83–91.

[10]Dosch, J., Leo, D., and Inman, D., "Modeling and Control for Vibration Suppression of a Flexible Active Structure," *Journal of Guidance, Control, and Dynamics*, Vol. 18, No. 2, 1995, pp. 340–346.

[11]Lin, C. Y., Crawley, E. F., and Heeg, J., "Open- and Closed-Loop Results of a Strain-Actuated Active Aeroelastic Wing," *Journal of Aircraft*, Vol. 33, No. 5, 1996, pp. 987–994.

[12]Bronowicki, A. J., Abhyankar, N. S., and Griffin, S. F., "Active Vibration Control of Large Optical Space Structures," *Smart Materials and Structures*, Vol. 8, No. 6, 1999, pp. 740–752.

[13]Vaillon, L., Petitjean, B., and Lebihan, D., "Active Isolation in Space Truss Structures: From Concept to Implementation," *Smart Materials and Structures*, Vol. 8, No. 6, 1999, pp. 781–790.

[14]Inman, D. J., *Engineering Vibration*, 2nd ed., Prentice–Hall, Upper Saddle River, NJ, 2001, pp. 510–512.

[15]Spencer, B. F., Jr., Suhardjo, J., and Sain, M. K., "Frequency Domain Optimal Control Strategies for Aseismic Protection," *Journal of Engineering Mechanics*, Vol. 120, No. 1, 1994, pp. 135–159.

[16]Friedland, B., *Control System Design: An Introduction to State Space Methods*, McGraw–Hill, New York, 1986, pp. 337–377.

[17]Franklin, G. F., Powell, J. D., and Emami-Naeini, A., *Feedback Control of Dynamic Systems*, 4th ed., Prentice–Hall, Upper Saddle River, NJ, 2002, pp. 541–548.

[18]Brennan, M. C., and McGowan, A. R., "Piezoelectric Power Requirements for Active Vibration Control," *Proceedings of the SPIE—The International Society for Optical Engineering*, Vol. 3039, Society of Photo-Optical Instrumentation Engineers (International Society for Optical Engineering), Bellingham, WA, 1997, pp. 660–669.

[19]Pausley, M. E., "Active Vibration Control of Space Structures During Space Shuttle Liftoff," M.S. Thesis, Dept. of Mechanical and Aeronautical Engineering, Clarkson Univ., Potsdam, NY, Dec. 2001.

M. P. Nemeth
Associate Editor